IET Generation, Transmission & Distribution

Research Article

IET Journals
The Institution of Engineering and Technology

Coordination of multi-type FACTS for available transfer capability enhancement using PI–PSO

ISSN 1751-8687
Received on 12th May 2020
Revised 30th June 2020
Accepted on 30th July 2020
E-First on 25th September 2020
doi: 10.1049/iet-gtd.2020.0886
www.ietdl.org

Ahmad Abubakar Sadiq[1] ✉, Muhammad Buhari[2], Sunusi Sani Adamu[2], Haruna Musa[3]

[1]*Electrical and Electronics Engineering, Federal University of Technology, P.M.B 65, Minna, Nigeria*
[2]*Electrical Engineering, Bayero University Kano, Kano, Nigeria*
[3]*Mechatronics Engineering, Bayero University Kano, Kano, Nigeria*
✉ *E-mail: ahmad.abubakar@futminna.edu.ng*

Abstract: To relieve congestion due to open-access feature in competitive power system framework, utilities plan flexible alternating current transmission systems (FACTS), ensuring improved utilization and performance of the transmission infrastructure. However, high-investment cost restricts implementation to single type of FACTS' planning in a time. Therefore, successive planning of another FACTS to delay transmission expansion results in multi-type FACTS planning. Consequently, to optimise performance, subsequent planning must coordinate with existing FACTS. The main objective of this study is to implement coordination of multi-type FACTS for available transfer capability (ATC) enhancement. A hybrid real power flow performance index (PI) and particle swarm optimisation (PSO), coordinate thyristor control series compensator (TCSC) in the first planning horizon with static synchronous series compensator (SSSC) and unified power flow controller (UPFC), in the second horizon. The PI–PSO-based multi-type FACTS coordination improves ATC of multilateral power transfers in a standard 9-buses test network. Results show that multi-type FACTS achieved higher ATC; such that enhanced ATC by TCSC–SSSC ranges between 8.06–69.34% while the TCSC–UPFC ranges between 11.85–71.59% for various power transfer transactions. A comparison of the three coordination schemes shows that the scheme with more decision parameters provides superior loadability and transfer capability improvement.

1 Introduction

Open access to the transmission grid, a feature of deregulation, ensures competition amongst utilities; whereas the ability to accurately evaluate available transfer capability (ATC) of the network to accommodate a high volume of power transactions, and to ensure power system's security is of significant concern [1–3]. The open-access feature can cause power flow overloads and congestion if not adequately managed, which may lead to instability [4].

The difficulties in acquiring the right ways for transmission lines, coupled with economic and regulatory constraints, may cause a reduction in power systems' operational margins, such as stability margins, voltage limits, and generator reactive power limits. On the other hand, improved transfer capability of existing transmission infrastructure may increase the risk of cascading outages in the presence of unmanaged power transactions [5–7]. The efficient utilisation of the existing transmission infrastructure is sort after by utilities. A common approach reported in the literature is the optimal deployment of flexible alternating current transmission systems (FACTS) devices [8, 9]. FACTS is a technology-based solution that enables power flow rerouting using circuit parameters towards relieving line overload and congestion [10]. Conversely, the huge investment cost associated with FACTS practically constrained utilities to a single type of FACTS planning at a given time horizon [11]. However, subsequent planning must account for and coordinate with the existing FACTS with regard to location and sizing. Accordingly, multiple FACTS planning at different time horizons requires adequate coordination of decision parameters for improved performance [9, 12].

The literature is replete with optimal location and sizing of different types of FACTS devices aimed at diverse objectives. In [12], voltage stability enhancement is demonstrated by coordinated control of static var compensator (SVC) and thyristor control series compensator (TCSC); while Li *et al.* [13] illustrate the enhancement in small-signal stability by coordinated damping control of TCSC and static synchronous compensator (STATCOM). Also, Li *et al.* [8] presented the design and application of multiple VSCs. The focus of this study, however, is on the coordination of multi-type FACTS for transfer capability improvement. A generic GUI-based multi-type FACTS location tool was presented in [14], the multi-type optimal placement ignores the huge investment cost of FACTS and hence the required coordination for successive planning horizons. The authors of [15–19] present multiple SVCs and TCSCs and their combination to enhance ATC; since the same planning horizon is assumed, SVC and TCSC's coordination was ignored. Jamnani and Pandya [19] refer to the simultaneous planning of SVC and TCSC as coordination. Similarly, Li *et al.* [10] present the combination of TCSC and SVC to minimise line power flow-based entropy. The term coordination therein implies the simultaneous optimal number of each FACTS. In the same vein, Nadeem *et al.* [20] demonstrated the concurrent optimal planning and coordination of TCSC, SVC, and unified power flow controller (UPFC) using whale optimisation; the coordination, however, is between FACTS and other reactive power control sources such as generators and transformer tap changers. In [21], total transfer capability (TTC) enhancement is demonstrated with multi-type FACTS consisting of TCSC, thyristor controlled phase shifter (TCPS), SVC, and UPFC simultaneously, which is rare in practice. Also, Elmitwally and Eladl [11] proposed an approach to allocating multi-type FACTS within the same time horizon. ATC enhancement with multiple STATCOM, static synchronous series compensator (SSSC), and UPFC separately was demonstrated in [22] under the same time horizon. Furthermore, Sadiq *et al.* [23] illustrated the coordination of SSSC with an existing TCSC in successive planning horizon. In addition to TCSC–SSSC coordination, this paper demonstrates the coordination of TCSC–UPFC using performance index (PI)–particle swarm optimisation (PSO)-based FACTS location and sizing; which is an extension of the work presented in [23].

Planning of many FACTS controllers requires the coordination of their locations and sizes. Every two FACTS' planning involves the coordination of at least four decision parameters. However, many FACTS' planning within the same time horizon is rare, and

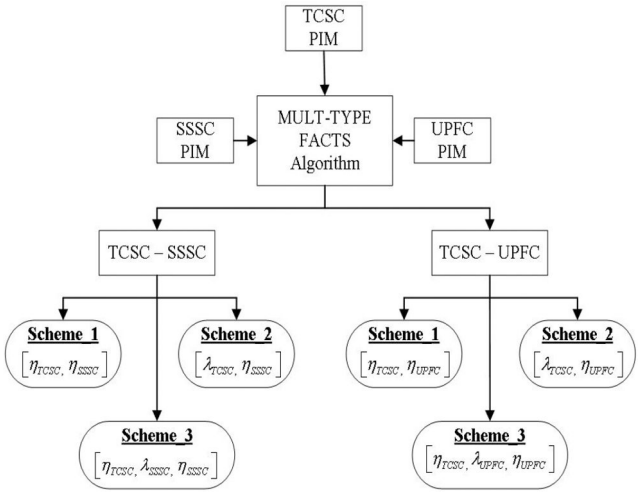

Fig. 1 *Schematic of multi-type FACTS coordination algorithm*

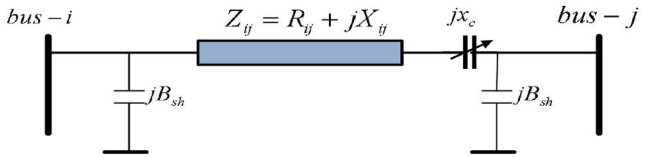

Fig. 2 *Transmission line model with TCSC [23]*

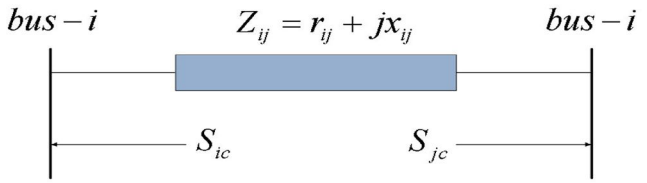

Fig. 3 *PIM of TCSC [23]*

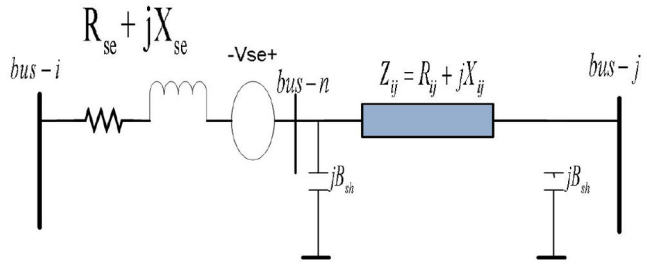

Fig. 4 *Equivalent VSC-based model of SSSC [23]*

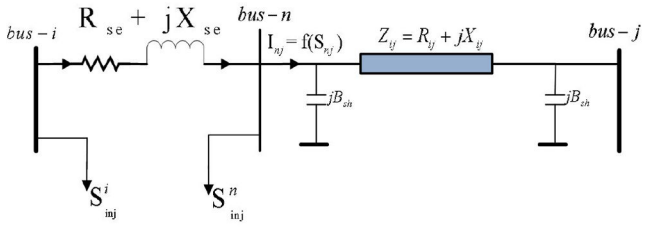

Fig. 5 *PIM of SSSC [23]*

successive time horizon is the practice. The key objective of this work is to demonstrate the coordination of multiple FACTS devices to improve ATC. The implementation of a hybrid real power flow PI and PSO is demonstrated herein, to locate and coordinate SSSC and UPFC each in the second planning horizon with an existing TCSC in the first horizon.

For each given planning horizon, a FACTS device allows two degrees of freedom as a decision parameter viz. location and size. In practice, however, for a successive time horizon, the bulkiness of FACTS reduces the degree of freedom by one, which is the location of the existing FACTS. The approach described in this paper differs from multiple FACTS planning at the same time horizon, which ignores coordination with the existing FACTS' size. This study demonstrates the coordination of SSSC and UPFC with an existing TCSC and subsequently compares three coordination scenarios under the successive planning horizon. Fig. 1 depicts the schematic of the multi-type algorithm with three coordination scenarios of SSSC and UPFC with an existing TCSC planned using PI–PSO under successive planning horizons. The multi-type FACTS coordination algorithm takes as input the power injection models (PIMs) of the various FACTS considered.

The rest of the paper is organised in sections as follows: Section 2 carefully describes the models of FACTS devices used. The location of FACTS using the sensitivities of real power flow with respect to FACTS' control parameter is described in Section 3, while Section 4 briefly documents the continuation power flow approach to ATC assessment. Also, Section 5 outlined the hybrid PI–PSO for ATC enhancement with FACTS, while some probable coordination scenarios under successive planning horizons were described in Section 6. Lastly, Section 7 present the results and discussions while concluding remarks are given in Section 8.

2 Static modelling of FACTS

2.1 TCSC modelling

A transmission line with TCSC is depicted in Fig. 2 and modelled by an equivalent reactance jx_k. Equation (1) describes the equivalent line reactance with TCSC

$$x_{ij}^{\text{new}} = x_{ij}^{\text{old}} - x_k \tag{1}$$

Complex power injections at the transmission lines terminal buses represent the TCSC' static model. Fig. 3 depicts the PIM of TCSC at the line of insertion. Equations (2)–(7) describe the power injections as well as the changes in conductance and susceptance. δ_{ij} is the voltage angular difference between the ith and jth buses; $\Delta Y_{ij} = \Delta G_{ij} + \Delta B_{ij}$ is the line admittance [24]

$$P_{ic} = V_i^2 \Delta G_{ij} - V_i V_j (\Delta G_{ij} \cos\delta_{ij} + \Delta B_{ij} \sin\delta_{ij}) \tag{2}$$

$$Q_{ic} = -V_i^2 \Delta B_{ij} - V_i V_j (\Delta G_{ij} \sin\delta_{ij} - \Delta B_{ij} \cos\delta_{ij}) \tag{3}$$

$$P_{jc} = V_j^2 \Delta G_{ij} - V_j V_i (\Delta G_{ij} \cos\delta_{ij} - \Delta B_{ij} \sin\delta_{ij}) \tag{4}$$

$$Q_{jc} = -V_j^2 \Delta B_{ij} + V_j V_i (\Delta G_{ij} \sin\delta_{ij} + \Delta B_{ij} \cos\delta_{ij}) \tag{5}$$

$$\Delta G_{ij} = \frac{x_k r_{ij} (x_k - 2x_{ij})}{(r_{ij}^2 + x_{ij}^2)(r_{ij}^2 + (x_{ij} - x_k)^2)} \tag{6}$$

$$\Delta B_{ij} = \frac{-x_k (r_{ij}^2 - x_{ij}^2 + x_k x_{ij})}{(r_{ij}^2 + x_{ij}^2)(r_{ij}^2 + (x_{ij} - x_k)^2)} \tag{7}$$

2.2 SSSC modelling

The equivalent SSSC circuit is shown in Fig. 4, which models' the SSSC by a voltage source $V_{se}\angle\delta_{se}$ connected in series with lossy transformer impedance Z_{se} to account for coupling losses. The PIM equivalent of SSSC, applying Norton equivalent, is modelled by complex loads at buses i and n as shown in Fig. 5; (8) and (9) give the SSSC's complex power injections [25].

$$S_{\text{inj}}^{i} = P_{\text{inj}}^{ic} + \text{j}Q_{\text{inj}}^{ic} = \overline{V_i}(I_{\text{inj}})^* \tag{8}$$

$$S_{\text{inj}}^{n} = P_{\text{inj}}^{n} + \text{j}Q_{\text{inj}}^{n} = -\overline{V_n}(I_{\text{inj}})^* \tag{9}$$

2.3 UPFCC modelling

For the UPFC, the voltage source converter (VSC) representation gives the operating principles and is depicted in Fig. 6. From the voltage source representation, Fig. 7 establishes and shows the UPFC's equivalent circuit connection in a transmission line [26,

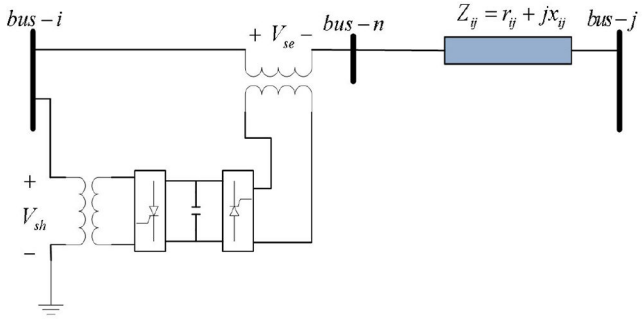

Fig. 6 *Voltage source operating principle of UPFC*

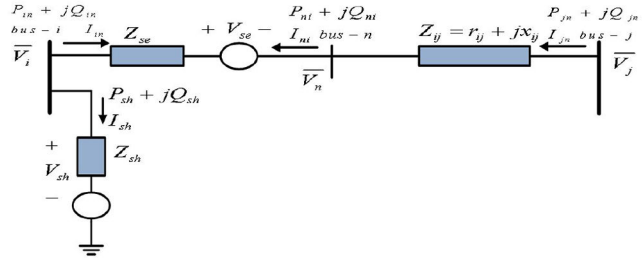

Fig. 7 *Equivalent VSC circuit of UPFC*

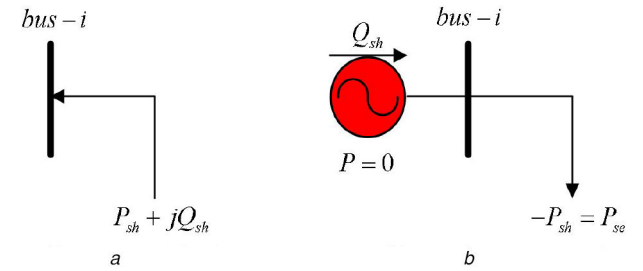

Fig. 8 *Equivalent shunt converter of UPFC*
(a) PIM model of STATCOM, ***(b)*** Synchronous condenser

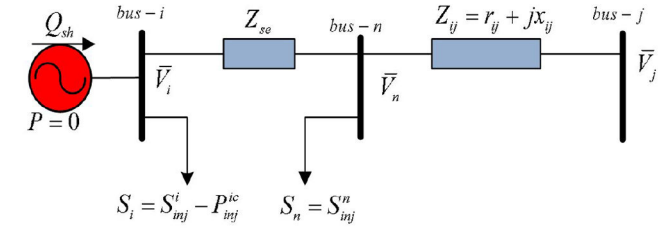

Fig. 9 *Power injection model of UPFC*

27]. In Fig. 7, the complex voltages $\bar{V}_{se}$ and $\bar{V}_{sh}$ are the injected series and controllable shunt parameters of the UPFC, while Z_{sh} and Z_{se} are the corresponding coupling transformer impedances, respectively. $\bar{V}_i$, $\bar{V}_j$, and $\bar{V}_n$ are the complex voltages at bus-*i* (sending end of the line), bus-*n* (UPFC's auxiliary bus) and bus-*j* (receiving end), respectively. These voltages in the rectangular form are defined by (10) while the active and reactive power flow equations with UPFC are given in (11)–(16) [28].

$$\left.\begin{aligned}
\bar{V}_{sh} &= V_{sh}\angle\delta_{sh} = V_{sh}(\cos\delta_{sh} + j\sin\delta_{sh})\\
\bar{V}_{se} &= V_{se}\angle\delta_{se} = V_{se}(\cos\delta_{se} + j\sin\delta_{se})\\
\bar{V}_i &= V_i\angle\delta_i = V_i(\cos\delta_i + j\sin\delta_i)\\
\bar{V}_n &= V_n\angle\delta_n = V_n(\cos\delta_n + j\sin\delta_n)\\
\bar{V}_j &= V_j\angle\delta_j = V_j(\cos\delta_j + j\sin\delta_j)
\end{aligned}\right\} \tag{10}$$

$$\begin{aligned}
P_{in}^{u} = {} & V_i^2 G_{in} - V_i V_n(G_{in}\cos\delta_{in} + B_{in}\sin\delta_{in})\\
& - V_i V_{se}(G_{in}\cos(\delta_i - \delta_{se}) + B_{in}\sin(\delta_i - \delta_{se}))
\end{aligned} \tag{11}$$

$$\begin{aligned}
Q_{in}^{u} = {} & -V_i^2 G_{in} - V_i V_n(G_{in}\sin\delta_{in} - B_{in}\cos\delta_{in})\\
& - V_i V_{se}(G_{in}\cos(\delta_i - \delta_{se}) - B_{in}\sin(\delta_i - \delta_{se}))
\end{aligned} \tag{12}$$

$$\begin{aligned}
P_{ni}^{u} = {} & V_n^2 G_{in} - V_i V_n(G_{in}\cos\delta_{in} + B_{in}\sin\delta_{in})\\
& + V_n V_{se}(G_{in}\cos(\delta_n - \delta_{se}) + B_{in}\sin(\delta_n - \delta_{se}))
\end{aligned} \tag{13}$$

$$\begin{aligned}
Q_{ni} = {} & -V_n^2 G_{in} - V_i V_n(G_{in}\cos\delta_{in} - B_{in}\sin\delta_{in})\\
& + V_n V_{se}(G_{in}\cos(\delta_n - \delta_{se}) - B_{in}\sin(\delta_n - \delta_{se}))
\end{aligned} \tag{14}$$

$$\begin{aligned}
P_{sh}^{u} = {} & V_i^2 G_{sh} - V_i V_{sh}(G_{sh}\cos(\delta_i - \delta_{sh})\\
& + B_{sh}\sin(\delta_i - \delta_{sh}))
\end{aligned} \tag{15}$$

$$\begin{aligned}
Q_{sh}^{u} = {} & -V_i^2 B_{sh} - V_i V_{sh}(G_{sh}\sin(\delta_i - \delta_{sh})\\
& - B_{sh}\cos(\delta_i - \delta_{sh}))
\end{aligned} \tag{16}$$

For the UPFC, an equivalent power injection can model the effect at the terminal buses of insertion [28], this approach treats the UPFC series branch similar to SSSC while the shunt branch as a compensator; STATCOM [27, 29]. The power injections due to the series branch of the UPFC are similar to (11)–(16) of the SSSC, while Fig. 8 shows the PIM of the UPFC's shunt converter [30].

Equation (17) expresses the active and reactive power injections resulting from the UPFC's shunt converter. The real and imaginary components of (17) simplify, similar to (15) and (16)

$$S_{sh}^{iu} = P_{sh}^{u} + Q_{sh}^{u} = \bar{V}_i I_{sh}^{*} = \bar{V}_i(\bar{V}_i^{*} - \bar{V}_{sh}^{*})Y_{sh}^{*} \tag{17}$$

Fig. 9 shows the complete PIM of UPFC obtained by combining the series converter model (SSSC) of Fig. 5 and the shunt converter model (STATCOM) of Fig. 8*b*. The real and reactive power injections at the UPFC's shunt, bus-*i* are expressed by (18)–(21), while the real and reactive power injections at the UPFC's auxiliary, bus-*n* are represented by (22) and (23), respectively

$$P_{inj}^{iu} = P_{inj}^{ic} + P_{sh}^{u} \tag{18}$$

$$\begin{aligned}
P_{inj}^{iu} = {} & V_i V_{se}[G_{se}\cos(\delta_i - \delta_{se}) + B_{se}\sin(\delta_i - \delta_{se})] + V_i^2 G_{sh}\\
& - V_i V_{sh}[G_{sh}\cos(\delta_i - \delta_{sh}) + B_{in}\sin(\delta_i - \delta_{sh})]
\end{aligned} \tag{19}$$

$$Q_{inj}^{iu} = Q_{inj}^{ic} + Q_{sh}^{u} \tag{20}$$

$$\begin{aligned}
Q_{inj}^{iu} = {} & -V_i V_{se}[G_{se}\sin(\delta_i - \delta_{se}) - B_{se}\cos(\delta_i - \delta_{se})] - V_i^2 B_{sh}\\
& - V_i V_{sh}[G_{sh}\sin(\delta_i - \delta_{sh}) - B_{sh}\cos(\delta_i - \delta_{sh})]
\end{aligned} \tag{21}$$

$$\begin{aligned}
P_{inj}^{nu} = P_{inj}^{nc} = {} & - V_n V_{se}[G_{se}\cos(\delta_n - \delta_{se})]\\
& - V_n V_{se}[B_{se}\sin(\delta_n - \delta_{se})]
\end{aligned} \tag{22}$$

$$\begin{aligned}
Q_{inj}^{nu} = Q_{inj}^{jc} = {} & V_n V_{se}[G_{se}\sin(\delta_n - \delta_{se})]\\
& - V_n V_{se}[B_{se}\cos(\delta_n - \delta_{se})]
\end{aligned} \tag{23}$$

For a given shunt converter's apparent power injection S_{sh}, the shunt converter voltage $\bar{V}_{sh}$ is shown in (24)

$$\bar{V}_{sh} = \bar{V}_i + Z_{sh}\left(\frac{S_{sh}}{\bar{V}_i}\right) \tag{24}$$

Equation (25) provides the necessary operating condition of a zero net active power exchange between the two UPFC's converters

$$\left.\begin{aligned}
\Delta P_{net} &= \mathrm{PE}_{sh} - \mathrm{PE}_{se} = 0\\
\mathrm{PE}_{sh} &= \mathrm{Re}(V_{sh} I_{sh}^{*})\\
\mathrm{PE}_{se} &= \mathrm{Re}(V_{se} I_{ni}^{*})
\end{aligned}\right\} \tag{25}$$

From the PIM models of TCSC, SSSC, and UPFC, the controllable parameters of each FACTS enable power flow

redistribution thereby relieving power flow congestion. Consequently, a choice of the suitable transmission line for FACTS is determined next to enhance ATC.

3 Sensitivity of real power flow index

Power flow congestion majorly constraints the power transfer [31]; hence, the changes in power flow to variations in circuit parameter as a result of FACTS control operations are used as a measure of the suitability of FACTS location, thereby allowing power flow redistribution to relieve congestion. Since power flow congestion is considered the major limitation to power transfers, while the second-order sensitivity is commonly used as a measure of severity of power flow overload, therefore, the sensitivity of the second-order real power flow performance indices ($\partial \mathrm{PI}_2$), is used for the determination of FACTS' location to improve ATC. Equation (26) describes the second-order real power flow performance indices (PI_2). Thus, for power transfer transactions constrained by flow limits, (27) evaluates the sensitivity of PI_2 concerning FACTS' control parameters (X_{FACTS}) [32]

$$\mathrm{PI}_2 = \sum_{m=1}^{N_\mathrm{L}} \frac{w_m}{2n}\left(\frac{P_{lm}}{P_{lm}^{\max}}\right)^{2n} \tag{26}$$

$$\frac{\partial \mathrm{PI}_2}{\partial X_{\mathrm{facts}}} = \sum_{m=1}^{N_\mathrm{L}} w_m P_{lm}^{(2n-1)}\left(\frac{1}{P_{lm}^{\max}}\right)^{2n} \frac{\partial P_{lm}}{\partial X_{\mathrm{facts}}} \tag{27}$$

where N_L is the number of lines, $w_m = 1$ is the non-negative weight coefficient used to reflect the importance of the line, n is the n-exponent order, P_{lm} is active power flow, and $P^{\max}$ is the rated capacity of the line. Equation (28) expresses the active power flow P_{lm} as the sum of real power injections [24]

$$P_{lm} = \begin{cases} \sum_{n=1, n\neq s}^{nb} S_{mn} P_n & \text{for } m \neq k \\ \sum_{n=1, n=s}^{nb} S_{mn} P_n + P_j & \text{for } m = k \end{cases} \tag{28}$$

where s is the slack bus, nb is the number of buses in the network, S_{mn} is the mnth element of the matrix $[\boldsymbol{S}_f]$ that relates line power flows with bus power injections at the buses without FACTS. Equation (29) expresses the partial derivative of the active power flow of (28) [32]

$$\frac{\partial P_{lm}}{\partial X_k} = \begin{cases} \left(S_{mi}\frac{\partial P_i}{\partial X_k} + S_{mj}\frac{\partial P_j}{\partial X_k}\right), & \text{for } m \neq k \\ \left(S_{mi}\frac{\partial P_i}{\partial X_k} + S_{mj}\frac{\partial P_j}{\partial X_k}\right) + \frac{\partial P_j}{\partial X_k} & \text{for } m = k \end{cases} \tag{29}$$

For TCSC, the derivative terms in (29) are the partial derivatives of (2) and (4), which models the TCSC as power injections. Equations (30)–(33) express the derivative with respect to TCSC's reactance

$$\left.\frac{\partial P_i}{\partial X_k}\right|_{x_k=0} = \left.\frac{\partial P_{ic}}{\partial x_k}\right|_{x_k=0} = (V_i^2 - V_i V_j \cos\delta_{ij})\left.\frac{\partial \Delta G_{ij}}{\partial X_k}\right|_{x_k=0} - (V_i V_j \sin\delta_{ij})\left.\frac{\partial \Delta B_{ij}}{\partial X_k}\right|_{x_k=0} \tag{30}$$

$$\left.\frac{\partial P_j}{\partial X_k}\right|_{x_k=0} = \left.\frac{\partial P_{jc}}{\partial x_k}\right|_{x_k=0} = (V_j^2 - V_i V_j \cos\delta_{ij})\left.\frac{\partial \Delta G_{ij}}{\partial X_k}\right|_{x_k=0} + (V_i V_j \sin\delta_{ij})\left.\frac{\partial \Delta B_{ij}}{\partial X_k}\right|_{x_k=0} \tag{31}$$

$$\left.\frac{\partial \Delta G_{ij}}{\partial x_k}\right|_{x_k=0} = 2G_{ij}B_{ij} \tag{32}$$

$$\left.\frac{\partial \Delta B_{ij}}{\partial x_k}\right|_{x_k=0} = B_{ij}^2 - G_{ij}^2 \tag{33}$$

In the case of SSSC, the derivative terms in (29) are the partial derivatives of the real parts of (8) and (9), which model the SSSC as power injections. Equations (34) and (35) give the derivative with respect to the magnitude of the series injected voltage of SSSC

$$\left.\frac{\partial P_i}{\partial X_k}\right|_{x_k=0} = \left.\frac{\partial P_{\mathrm{inj}}^{ic}}{\partial V_{\mathrm{se}}}\right|_{V_{\mathrm{se}}=0} = V_i[G_{\mathrm{se}}\cos(\delta_i + \delta_{\mathrm{se}})] - V_i[B_{\mathrm{se}}\sin(\delta_i + \delta_{\mathrm{se}})] \tag{34}$$

$$\left.\frac{\partial P_j}{\partial X_k}\right|_{x_k=0} = \left.\frac{\partial P_{\mathrm{inj}}^{nc}}{\partial V_{\mathrm{se}}}\right|_{V_{\mathrm{se}}=0} = -V_n[G_{\mathrm{se}}\cos(\delta_n + \delta_{\mathrm{se}})] - V_i[B_{\mathrm{se}}\sin(\delta_n + \delta_{\mathrm{se}})] \tag{35}$$

For the UPFC, the terms $(\partial P_i/\partial X_k)|_{x_k=0}$ and $(\partial P_j/\partial X_k)|_{x_k=0}$ are obtained from partial differentials of (18)–(23), which are given by (36)–(39), respectively

$$\left.\frac{\partial P_{\mathrm{inj}}^{iu}}{\partial V_{\mathrm{se}}^{u}}\right|_{V_{\mathrm{se}}=0} = V_i[G_{\mathrm{se}}\cos(\delta_i - \delta_{\mathrm{se}}) + B_{\mathrm{se}}\sin(\delta_i - \delta_{\mathrm{se}})] \tag{36}$$

$$\left.\frac{\partial Q_{\mathrm{inj}}^{iu}}{\partial V_{\mathrm{se}}^{u}}\right|_{V_{\mathrm{se}}=0} = -V_i[G_{\mathrm{se}}\sin(\delta_i - \delta_{\mathrm{se}}) - B_{\mathrm{se}}\cos(\delta_i - \delta_{\mathrm{se}})] \tag{37}$$

$$\left.\frac{\partial P_{\mathrm{inj}}^{nu}}{\partial V_{\mathrm{se}}^{u}}\right|_{V_{\mathrm{se}}=0} = -V_n[G_{\mathrm{se}}\cos(\delta_n + \delta_{\mathrm{se}}) - B_{\mathrm{se}}\sin(\delta_n + \delta_{\mathrm{se}})] \tag{38}$$

$$\left.\frac{\partial Q_{\mathrm{inj}}^{nu}}{\partial V_{\mathrm{se}}^{u}}\right|_{V_{\mathrm{se}}=0} = V_n V_{\mathrm{se}}[G_{\mathrm{se}}\sin(\delta_n + \delta_{\mathrm{se}}) + B_{\mathrm{se}}\cos(\delta_n + \delta_{\mathrm{se}})] \tag{39}$$

Alternatively, the partial derivative of active power flows in (29) can be approximated from the first principle [33] using

$$\frac{\partial P_{lm}}{\partial X_k} = \lim_{x_k \to 0} \frac{P_{lm}(x_{ij} + x_k) - P_{lm}(x_{ij})}{\Delta x_k} \tag{40}$$

Note that in (30)–(39), the sensitivities are obtained by assuming that $X_{\mathrm{FACTS}} \to 0$.

Upon evaluating the sensitivities of FACTS' controlled parameter to each power transfer transaction, an assessment of the ATC objective term is obtained. In [34], the comparative advantages of various ATC assessment approaches were documented.

4 Continuation power flow (CPF)

The CPF is a predictor–corrector scheme that varies load and generation simultaneously by a loading parameter λ used to parameterise the load flow equations. The parameterised load flow procedure of CPF avoids ill-conditioning and singularity. The high accuracy and efficiency of CPF make it one of the widely used methods for static security assessment [35].

The comprehensive documentation of CPF for ATC evaluation and enhancement with FACTS are given in [34, 36–38]. The assessment of enhanced ATC with FACTS due to the imposed constraints formulates to an optimisation objective, and at the maximum loading parameter, the ATC is evaluated as [39]

$$\max\left\{\mathrm{ATC} = \sum_{i\in \mathrm{sink}} P_{\mathrm{L}}^{i}(\lambda_{\mathrm{limited}}) - \sum_{i\in \mathrm{sink}} P_{\mathrm{L}}^{i}(\lambda = 0)\right\} \tag{41}$$

Subject to

$$f(x, \lambda) = 0 \tag{42}$$

$$0 \le \lambda \le \lambda_{\text{limited}} \tag{43}$$

$$P_{\text{g}}^{\min} \le P_{\text{g}} \le P_{\text{g}}^{\max} \tag{44}$$

$$Q_{\text{g}}^{\min} \le Q_{\text{g}} \le Q_{\text{g}}^{\max} \tag{45}$$

$$S_{ij} \le S_{ij}^{\text{rated}} \tag{46}$$

$$V_i^{\min} \le V_i \le V_i^{\max} \tag{47}$$

$$X_{\text{FACTS}}^{\min} \le X_{\text{FACTS}} \le X_{\text{FACTS}}^{\max} \tag{48}$$

Equation (42) is the non-linear compact power flow equation, with state variable $x = (V; \delta)$ as voltage magnitude and angle. In (43)–(47), λ_{limited}, P_{g}, Q_{g}, S_{ij}, and V_i are loading parameter, real, reactive, apparent power flows, and voltage magnitude, respectively. Equation (48) ensures minimum FACTS' size,which is treated as a constraint and imposed by X_{FACTS}; $-0.8 \le X_{\text{TCSC}} \le 0.2$ for TCSC, and $0 \le X_{\text{SSSC}}^{\text{Vse}} \le 0.1$ for SSSC, $0 \le X_{\text{UPFC}}^{\text{Vse}} \le 0.1$ for the series branch, while the equivalent shunt converter maintains the shunt bus voltage of the UPFC at $0.9 \le X_{\text{UPFC}}^{\text{Vsh}} \le 1.09$, respectively.

5 Hybrid PI and PSO (PI–PSO)

The criteria to obtained the reduced search space are detailed in [23, 34]. In the PI–PSO implementation detailed in [34], ∂PI obtains a vector of likely candidate location of FACTS within which PSO optimises the size, thereby improving the overall algorithm's exploitation ability and avoid local optimal solutions. Equation (49) describes the particle's position, such that λ and X are location and size, respectively. For an m-dimension vector of candidate location, in addition to position and velocity updates of (50) and (51), respectively, in conventional PSO, position update in PI–PSO [34] is described in (52)

$$\eta_i^k = \left[\lambda_i^k, X_i^k\right] \tag{49}$$

$$\eta_i^{k+1} = \eta_i^k + V_i^{k+1} \tag{50}$$

$$\begin{aligned} V_i^{k+1} = {} & \omega V_i^k + c_1 \text{rand}(\text{Pbest}_i^k - \eta_i^k) \\ & + c_2 \text{rand}(\text{Gbest}_i^k - \eta_i^k) \end{aligned} \tag{51}$$

$$X_i^{k+1} = \begin{cases} X_i^{k+1}(\lambda_i) & \text{if } \lambda_i^{k+1} \in \mathbb{N} \\ \mathbb{N}(\text{randperm}(m, 1)) & \text{if } \lambda_i^{k+1} \notin \mathbb{N} \\ X_i^{k+1}(\eta_i) & \text{for } \eta_i \in \mathbb{R} \end{cases} \tag{52}$$

Therefore, PI–PSO differ from the PSO in the following: (i) ability to obtain a reduced search space, (ii) randomisation of the initial particles within the reduced search space and (iii) PI–PSO is constrained to only searches for an optimal solution within the reduced search space rather than the entire space by PSO. The flowchart of the typical hybrid PI–PSO for ATC enhancement with FACTS is depicted in Fig. 10

6 Coordination schemes

The term coordination implies that FACTS' decision parameters have been tuned simultaneously for an overall improvement of the objective. Herein, the multi-type FACTS coordination is targeted at ATC improvement. Coordination of SSSC or UPFC with an existing TCSC under successive time horizons requires the coordination of four decision parameters, namely $[\lambda_{\text{TCSC}}, X_{\text{TCSC}}, \lambda_{\text{SSSC}}, X_{\text{SSSC}}]$. Since many FACTS planning within the same time horizon is rare in practice, three coordination scenarios of SSSC or UPFC with an existing TCSC is illustrated using PI–PSO under successive planning horizons. As a strategy, multiple FACTS on the same location is precluded. The three coordination schemes are described as follows:

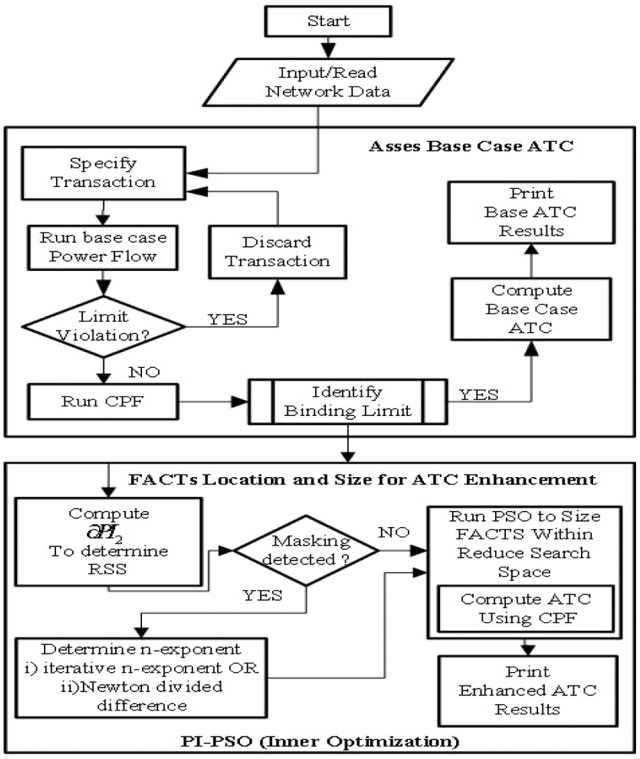

Fig. 10 *Typical flowchart of hybrid PI–PSO (source: [34])*

6.1 *Scheme*$_1$

In this scheme, sizes of FACTS η_{SSSC} and η_{UPFC} only coordinate with the variables λ_{TCSC} and η_{TCSC}. Locations of TCSC, SSSC, or UPFC optimally planned separately using PI–PSO are retained, while PSO optimises their sizes at these respective locations. Equation (53) gives the decision variables under *scheme*$_1$

$$\begin{cases} [\eta_{\text{TCSC}}, \eta_{\text{SSSC}}] & \text{for TCSC--SSSC} \\ [\eta_{\text{TCSC}}, \eta_{\text{UPFC}}] & \text{for TCSC--UPFC} \end{cases} \tag{53}$$

6.2 *Scheme*$_2$

Here, FACTS' location and sizes (λ_{SSSC} and η_{SSSC} or λ_{UPFC} and η_{UPFC}) coordinate with static TCSC's location and size (λ_{TCSC} and η_{TCSC}). The SSSC or UPFC's location and size are optimised in the presence of an optimally planned (location and size) TCSC separately using PI–PSO. Equation (54) gives the decision variables under *scheme*$_2$

$$\begin{cases} [\lambda_{\text{SSSC}}, \eta_{\text{SSSC}}] & \text{for TCSC--SSSC} \\ [\lambda_{\text{UPFC}}, \eta_{\text{UPFC}}] & \text{for TCSC--UPFC} \end{cases} \tag{54}$$

6.3 *Scheme*$_3$

Location and sizes of SSSC or UPFC (λ_{SSSC}, and η_{SSSC} or λ_{UPFC}, and η_{UPFC}) coordinate only with the variable size of TCSC. This scheme optimises the location and size of SSSC or UPFC as well as the size of a separately planned TCSC using PI–PSO. Equation (55) gives the decision variables

$$\begin{cases} [\eta_{\text{TCSC}}, \lambda_{\text{SSSC}}, \eta_{\text{SSSC}}] & \text{for TCSC-SSSC} \\ [\eta_{\text{TCSC}}, \lambda_{\text{UPFC}}, \eta_{\text{UPFC}}] & \text{for TCSC-UPFC} \end{cases} \tag{55}$$

7 Results and discussions

Fig. 11 depicts the one-line diagram of the Western System Coordinating Council (WSCC) 9 buses network obtained by a web-based network visualisation tool 'stac' (steady-state AC network visualisation in the browser). Detailed system parameters of the

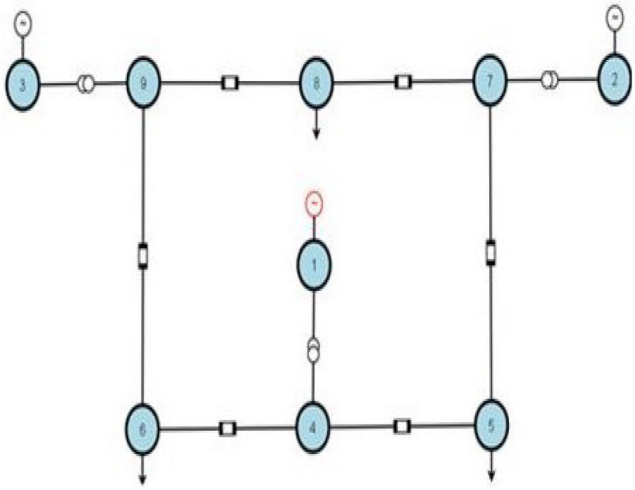

Fig. 11 *One-line diagram of WSCC 9 buses*

Table 1 Second-order sensitivity (∂PI_2) of PI to TCSC's reactance

Trans.			Line number(terminating buses)								
ID	Source	Sink	1(1–4)	2(4–5)	3(5–7)	4(2–7)	5(7–8)	6(8–9)	7(9–3)	8(9–6)	9(6–4)
T1	1, 3	5	0.0137	**−0.7046**	1.7751	0.0898	**−0.1183**	0.6834	−0.0484	**−0.9763**	−0.0192
T2	1, 2	5, 8	−0.0273	0.2582	**−0.5396**	−0.0268	0.9141	**−0.1696**	0.0368	0.4394	**−0.4586**
T3	1, 2, 3	5, 6	0.0772	0.0314	1.298	0.0765	**−0.3613**	0.0104	−0.0322	**−0.5668**	0.3071
T4	1, 2, 3	6, 8	−0.0696	**−0.1910**	**−0.4354**	−0.0201	0.8763	**−0.1804**	0.098	0.8005	**−0.6959**
T5	2, 3	5	0.0437	0.0677	1.4802	0.0726	**−0.4457**	0.0698	−0.0204	**−0.6223**	0.0711
T6	1	8	−0.0586	0.7089	**−0.1627**	0.0104	1.1636	**−1.0226**	−0.006	0.0126	**−1.5384**
T7	1, 2, 3	5, 8	0.0327	0.022	0.7473	0.0623	**−0.0046**	0.0209	0.0113	**−0.0078**	0.0048
T8	2, 3	6	0.0600	0.1719	1.1030	0.0663	**−0.2554**	**−0.0135**	−0.0235	**−0.4267**	0.198
T9	1, 2	8	−0.0343	**−0.1271**	**−0.6524**	−0.0193	1.1083	**−0.1430**	0.0375	0.5739	**−0.4826**
T10	1, 2	5, 6	0.0465	0.0258	0.6759	0.0413	**−0.0116**	0.0021	0.0086	**−0.0414**	**−0.007**

Table 2 Second-order sensitivity (∂PI_2) of PI to SSSC's series injected voltage

Trans.	Line number(terminating buses)								
ID	1(1–4)	2(4–5)	3(5–7)	4(2–7)	5(7–8)	6(8–9)	7(9–3)	8(9–6)	9(6–4)
T1	−0.057	3.4411	**−5.329**	0.5169	0.4379	**−3.3775**	−0.2709	5.117	0.0364
T2	0.0841	**−1.088**	4.6866	2.2759	**−3.5912**	0.9938	−0.097	**−1.9424**	2.554
T3	−0.2885	**−0.0964**	**−2.6338**	1.6763	2.5468	**−0.1333**	−0.0142	3.3301	**−1.3878**
T4	0.2544	1.0153	4.4098	2.4144	**−3.2473**	1.018	−0.3463	**−3.5896**	3.9137
T5	−0.1436	**−0.2564**	**−3.6751**	1.4946	2.8103	**−0.4357**	−0.0756	3.4646	**−0.3659**
T6	0.1269	**−3.1581**	1.3391	0.0615	**−6.7268**	5.5265	0.4957	0.3898	8.0399
T7	−0.1154	**−0.0411**	0.436	2.4735	1.2911	**−0.0552**	−0.1271	0.3864	**0.0022**
T8	−0.222	**−0.6847**	**−1.6413**	1.8837	2.2394	0.0266	−0.0811	2.887	**−0.8476**
T9	0.0842	0.7067	4.6791	1.9622	**−4.5912**	0.8256	−0.1232	**−2.5717**	2.6148
T10	−0.1783	**−0.0532**	0.7081	2.4452	1.1020	**−0.0309**	−0.0141	0.3635	0.557

test network are available in [12]. Several multilateral power transactions were simulated within MATPOWER environment [40]. Transfer directions of some transactions are described in the second and third column of Table 1.

In the first planning horizon, which optimally locate and size TCSC; the sensitivities of real power flow to TCSC's controlled parameters for each transaction are given in Table 1. Similarly, Tables 2 and 3 also provide the sensitivities with SSSC and UPFC, respectively. In Tables 1–3, the values in bold and their corresponding lines constitute the elements of the vector of potential candidate locations. The optimal solution of PI–PSO-based enhanced ATC with TCSC, SSSC, and UPFC separately is given by Table 4. From Table 4, observe that ATC improvement above the base case is achieved with the optimal location of TCSC, SSSC, and UPFC individually using PI–PSO.

Furthermore, for TCSC, SSSC, and UPFC, respectively, Figs. 12–14 depict the performance of the PI–PSO-based ATC enhancement in terms of improved exploitation ability over the conventional PSO, regarding the starting point, convergence to global optima, and superior ATC values.

From Fig. 12*a*, for a typical ATC enhancement with TCSC for transaction T2, the reduced search space feature in PI–PSO ensures an improved starting point of about 147 MW compared to PSO with 138 MW. A similar trend is equally observed in Fig. 12*b*. The improved starting point in Figs. 12*a* and *b* is attributed to the randomisation of the initial particles is within the reduced search space obtained by the sensitivities of the PI component of the PI–PSO.

For the convergence characteristics with SSSC in Figs. 13*a* and *b*, in addition to the improved starting point ability of PI–PSO in contrast, conventional PSO seems trapped into local optimal solutions, which results to PI–PSO obtaining her ATC of about 158 MW against 153 MW with PSO for transaction T7, and 178 MW against 174 MW with PSO for transaction T4. Also, from the convergence curve comparison with UPFC in Fig. 14*a*, although PSO and PI–PSO obtain similar ATC of about 68 MW for T5,

Table 3 Second-order sensitivity (∂PI_2) of PI to UPFC's series injected voltage

Trans. ID	Line number(terminating buses)								
	1(1–4)	2(4–5)	3(5–7)	4(2–7)	5(7–8)	6(8–9)	7(9–3)	8(9–6)	9(6–4)
T1	−0.057	3.5365	**−1.4064**	−0.1662	**−0.7599**	**−2.9091**	0.5857	5.3556	**−2.6177**
T2	0.0841	**−0.8981**	3.3095	0.051	**−4.2736**	1.913	−0.4851	**−2.2339**	2.6181
T3	−0.2885	0.4194	**−0.2021**	−0.1592	0.9364	**−0.1166**	0.2227	3.3305	**−1.807**
T4	0.2544	0.6025	2.5611	0.0366	**−4.0496**	2.6954	0.6637	**−2.8574**	5.0756
T5	−0.1436	**−0.4648**	**−1.7297**	−0.0987	0.2656	**−0.4113**	0.9979	4.3333	**−1.0893**
T6	0.1269	**−1.5431**	1.183	−0.0147	**−6.8351**	4.7505	0.0068	0.3952	5.1231
T7	−0.1154	**−0.0100**	**−0.2774**	−0.1781	0.3510	**−0.5488**	−0.0571	0.3082	**−0.6141**
T8	−0.2220	**−0.3692**	**−0.4048**	−0.1307	0.3742	**−0.0943**	0.1254	2.7699	**−1.0051**
T9	0.0842	1.6206	4.3933	0.0274	**−5.1316**	1.7044	−0.9824	**−3.2939**	2.7155
T10	−0.4016	1.4024	0.9428	−0.2171	2.4188	**−0.2970**	−0.0621	2.5064	**−0.2177**

Table 4 Enhanced ATC values with TCSC, SSSC, and UPFC using PI–PSO

Trans. ID	ATC, MW				SSSC's solution			TCSC's solution		UPFC's solution			
	Base case	UPFC only	SSSC only	TCSC only	Line no.	V_{se}, p.u.	δ_{se}, deg	Line no.	% comp	Line no.	V_{se}, p.u	δ_{se}, deg	Q_{sh}, MVAR
T1	143.25	220.26	166.58	182.04	6	0.088	158.75	8	80.00	3	0.100	92.64	167.72
T2	127.16	158.30	159.40	153.85	5	0.100	166.30	3	46.62	5	0.058	117.44	54.74
T3	118.02	173.20	143.09	172.64	3	0.051	−76.74	8	76.01	3	0.096	92.424	122.42
T4	155.14	187.32	176.08	181.07	8	0.058	61.81	3	38.96	8	0.029	−11.72	236.06
T5	43.63	68.00	64.84	64.40	3	0.055	43.98	8	80.00	3	0.100	83.25	26.29
T6	128.03	168.81	163.85	158.77	5	0.084	121.24	9	80.00	5	0.0380	−107.3	209.59
T7	138.64	157.63	158.55	151.88	3	0.100	−35.79	5	57.21	6	0.0330	42.28	99.06
T8	74.61	102.98	89.89	101.54	2	0.071	142.65	8	57.39	3	0.091	91.44	142.61
T9	60.29	83.32	88.32	79.59	5	0.1	172.54	3	65.37	5	0.013	−118.8	53.33
T10	159.46	178.89	169.95	172.05	2	0.056	73.56	8	35.06	9	0.067	−42.44	214.16

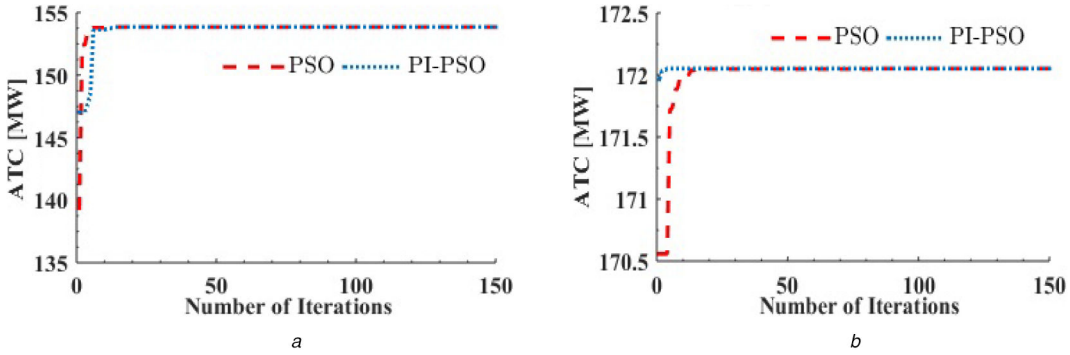

Fig. 12 *Convergence curve of PI–PSO over PSO with TCSC*
(a) Transaction T2 with TCSC, ***(b)*** Transaction T10 with TCSC

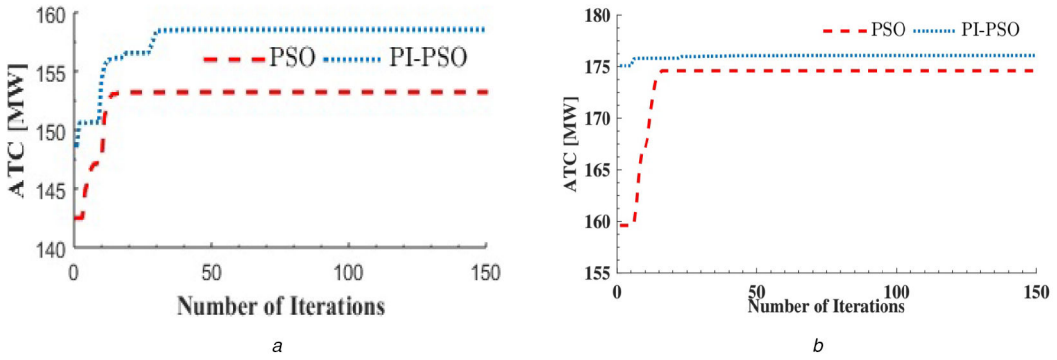

Fig. 13 *Convergence curve of PI–PSO over PSO with SSSC*
(a) Transaction T7 with SSSC, ***(b)*** Transaction T4 with SSSC

observe that the PI–PSO has improved starting point and converged to this optimal solution with about 30 iterations compared to PSO with over 50 iterations to convergence. For transaction T6 with UPFC, Fig. 14*b* depicts that the PI–PSO outperforms PSO under improved starting point, convergence to optimal ATC, and lesser number of iterations to convergence.

It is worthy to note that for a large power system network, the efficiency of the computation is germane. Both PSO and PI–PSO

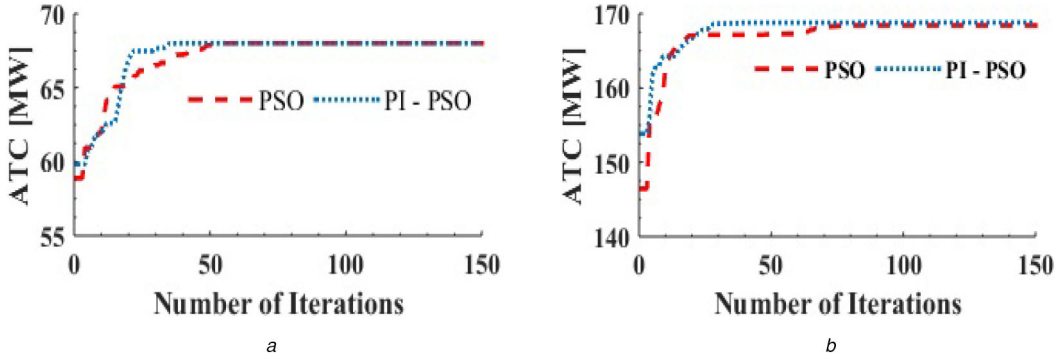

Fig. 14 *Convergence curve of PI–PSO over PSO with UPFC*
(a) Transaction T5 with UPFC, ***(b)*** Transaction T6 with UPFC

Table 5 Enhanced ATC values with TCSC–SSSC under coordination $Scheme_1$

Trans. ID	ATC, MW TCSC only	ATC, MW SSSC only	ATC, MW TCSC–SSSC	TCSC's solution Line no.	TCSC's solution % comp	SSSC's solution Line no.	SSSC's solution V_{se}, p.u	SSSC's solution δ_{se}, deg
T1	182.0445	166.5841	184.633	8(9–6)	**80**	6(8–9)	**0.1**	**−165.4583**
T2	153.8509	159.4050	153.9241	3(5–7)	**21.23**	5(7–8)	**0.1**	**132.9342**
T3	172.6368	143.0993	173.9017	8(9–6)	**54.295**	3(5–7)	**0.1**	**−44.775**
T4	181.0729	176.0799	179.1634	3(5–7)	**22.7756**	5(7–8)	**0.1**	**89.7476**
T5	64.4040	64.8441	73.8841	8(9–6)	**80**	3(5–7)	**0.1**	**−34.5029**
T6	158.7672	163.8505	171.9141	9(6–4)	**80**	5(7–8)	**0.1**	**19.9095**
T7	151.8813	158.5469	154.7324	5(7–8)	**63.5491**	6(8–9)	**0.1**	**−159.9218**
T8	101.5460	89.8998	102.9261	8(9–6)	**50.3745**	2(4–5)	**0.1**	**−18.8537**
T9	79.5977	88.3222	82.5282	3(5–7)	**36.5695**	5(7–8)	**0.1**	**131.7564**
T10	172.0520	169.9509	172.3073	8(9–6)	**17.0767**	3(5–7)	**0.1**	**−74.441**

Table 6 Enhanced ATC values with TCSC–SSSC under coordination $Scheme_2$

Trans. ID	ATC, MW TCSC only	ATC, MW SSSC only	ATC, MW TCSC-SSSC	TCSC's solution Line no.	TCSC's solution % comp	SSSC's solution Line no.	SSSC's solution V_{se}, p.u	SSSC's solution δ_{se}, deg
T1	182.0445	166.5841	199.7187	8(9–6)	80	**9(6–4)**	**0.1**	**16.6043**
T2	153.8509	159.4050	162.346	3(5–7)	46.6243	**4(2–7)**	**0.1**	**134.969**
T3	172.6368	143.0993	175.585	8(9–6)	76.0102	**6(8–9)**	**0.1**	**161.818**
T4	181.0729	176.0799	182.238	3(5–7)	38.9587	**6(8–9)**	**0.06898**	**−154.5**
T5	64.4040	64.8441	73.8841	8(9–6)	80	**3(5–7)**	**0.1**	**−34.507**
T6	158.7672	163.8505	172.88	9(6–4)	80	**3(5–7)**	**0.1**	−148.46
T7	151.8813	158.5469	154.693	5(7–8)	57.2176	**6(8–9)**	**0.1**	**−166.09**
T8	101.5460	89.8998	103.039	8(9–6)	57.3979	**6(8–9)**	**0.1**	**157.096**
T9	79.5977	88.3222	81.8093	3(5–7)	65.3655	**2(4–5)**	**0.05313**	**−106.14**
T10	172.0520	169.9509	175.216	8(9-6)	35.0626	**6(8–9)**	**0.1**	**165.127**

algorithms are executed on an Intel Core i3 computer with 4 GB RAM. The CPU time is expected to increase in the case of a real power system with a large number of buses, however, computers with higher and more efficient computing power are the answer to the real problems.

In the second planning horizon, where SSSC or UPFC coordinate with an existing TCSC, the enhanced ATC improvement with TCSC–SSSC and TCSC–UPFC coordination is given in Tables 5–10. In Tables 5–10, for each coordination scheme under the TCSC–SSSC and TCSC–UPFC, the optimal decision parameters involved in the coordination are shown in bold.

Tables 5–7 distinguish between coordination $schemes_1$, $schemes_2$ and $schemes_3$ for the TCSC–SSSC coordination, while Tables 8–10 outline the results of $schemes_1$, $schemes_2$ and $schemes_3$ with TCSC–UPFC coordination, respectively. The higher ATC obtained by TCSC–UPFC in Tables 8–10 compared to TCSC-SSSC in Tables 5–7, is attributed to the presence of the UPFC devices compared with the SSSC. Since the UPFC has two VSC at the line of insertion, the UPFC simultaneously impacts both the series and shunt branches as depicted in Fig. 7. Therefore, in addition to the injection by the series converter in the SSSC, the UPFC's shunt converter injection contributes to power flow redistribution and hence relief congestion and improve the voltage profile particularly at the shunt branch.

A comparison of enhanced ATC with single FACTS in Table 4 with the various coordination schemes in Tables 5–10 show that, while % enhancement in ATC by TCSC, SSSC, and UPFC is in the range of (7.89–47. 61%), (6.58–48. 62%), and (12.18–55.85%), respectively; the multi-type FACTS namely: TCSC–SSSC and TCSC–UPFC obtains improvement in the range of (8.06–69.34%) and (11.85–71.59%), respectively, for various power transfer transactions.

To compare the coordination schemes, Fig. 15 illustrates the convergence curve of transaction T3 with TCSC–SSSC under the three coordination schemes. From Tables 5–10 as well as Fig. 15, coordination $scheme_3$ obtains superior ATC improvement. Observe in Fig. 15 a higher number of iterations to convergence $scheme_3$, which is attributable to the additional number of decision

Table 7 Enhanced ATC values with TCSC-SSSC under coordination $Scheme_3$

Trans. ID	ATC, MW TCSC only	ATC, MW SSSC only	TCSC-SSSC	TCSC's solution Line no.	TCSC's solution % comp	SSSC's solution Line no.	SSSC's solution V_{se}, p.u	SSSC's solution δ_{se}, deg
T1	182.0445	166.5841	199.7187	8(9–6)	**80**	**9(6–4)**	**0.1**	**16.6043**
T2	153.8509	159.4050	163.2491	3(5–7)	**45.5584**	**4(2–7)**	**0.0999**	**133.5905**
T3	172.6368	143.0993	178.9711	8(9–6)	**69.5688**	**4(2–7)**	**0.1**	**107.7372**
T4	181.0729	176.0799	182.8320	3(5–7)	**57.0019**	**6(8–9)**	**0.0591**	**160.8116**
T5	64.4040	64.8441	73.8841	8(9–6)	**80**	**3(5–7)**	**0.1**	**−34.5068**
T6	158.7672	163.8505	172.8799	9(6–4)	**80**	**3(5–7)**	**0.1**	**−148.466**
T7	151.8813	158.5469	162.6633	5(7–8)	**35.7543**	**4(2–7)**	**0.1**	**120.0035**
T8	101.5460	89.8998	102.1398	8(9–6)	**80**	**6(8–9)**	**0.1**	**166.225**
T9	79.5977	88.3222	82.5277	3(5–7)	**36.0922**	**5(7–8)**	**0.1**	**132.9508**
T10	172.0520	169.9509	175.4393	8(9–6)	**53.5863**	**6(8–9)**	**0.1**	**175.6063**

Table 8 Enhanced ATC values with TCSC–UPFC under coordination $Scheme_1$

Trans. ID	ATC, MW TCSC only	ATC, MW UPFC only	TCSC-UPFC	TCSC's solution Line no.	TCSC's solution % comp	UPFC's solution Line no.	UPFC's solution V_{se}, p.u	UPFC's solution δ_{se}, deg	UPFC's solution V_{sh}, p.u	UPFC's solution δ_{sh}, deg	UPFC's solution Q_{sh} (MVAR)	UPFC's solution V_{sh}^{b}, p.u
T1	182.0445	220.262	226.5571	8(9–6)	**80**	3(5–7)	**0.09836**	**−83.653**	**1.1189**	**−12.288**	**129.4838**	**0.98779**
T2	153.8509	158.3029	158.3032	3(5–7)	**5.9031**	5(7–8)	**0.06365**	**103.479**	**1.0784**	**9.3979**	**54.7215**	**1.025**
T3	172.6368	173.2049	177.544	8(9–6)	**30.1327**	3(5–7)	**0.03714**	**106.055**	**1.1895**	**−3.4404**	**143.7602**	**1.0529**
T4	181.0729	187.3188	187.4227	3(5–7)	**13.6116**	8(9–6)	**0.05235**	**35.0213**	**1.2748**	**5.7007**	**216.4285**	**1.0731**
T5	64.404	68.0017	74.7289	8(9–6)	**72.8753**	3(5–7)	**0.05043**	**-31.718**	**1.0525**	**0.31049**	**64.2995**	**0.987**
T6	158.7672	168.8062	170.504	9(6–4)	**80**	5(7–8)	**0.0852**	**97.3978**	**1.2629**	**−9.2089**	**188.4457**	**1.09**
T7	151.8813	157.6258	157.613	5(7–8)	**34.6395**	6(8–9)	**0.04097**	**−42.742**	**1.1027**	**7.1354**	**87.6361**	**1.0165**
T8	101.546	102.9787	103.1231	8(9–6)	**31.5300**	3(5–7)	**0.04055**	**−69.186**	**1.0875**	**2.6058**	**70.0513**	**1.0187**
T9	79.5977	83.315	83.3166	3(5–7)	**8.9891**	5(7–8)	**0.0332**	**147.869**	**1.0643**	**14.9793**	**40.341**	**1.025**
T10	172.052	178.886	179.1264	8(9–6)	**24.0385**	9(6–4)	**0.09846**	**−72.082**	**1.2893**	**−9.7315**	**217.2736**	**1.09**

Table 9 Enhanced ATC values with TCSC–UPFC under coordination $Scheme_2$

Trans. ID	ATC, MW TCSC only	ATC, MW UPFC only	TCSC–UPFC	TCSC's solution Line no.	TCSC's solution % comp	UPFC's solution Line no.	UPFC's solution V_{se}, p.u	UPFC's solution δ_{se}, deg	UPFC's solution V_{sh}, p.u	UPFC's solution δ_{sh}, deg	UPFC's solution Q_{sh} (MVAR)	UPFC's solution V_{sh}^{b}, p.u
T1	182.0445	220.262	226.5577	8(9–6)	80	**3(5–7)**	**0.1**	**−93.3375**	**1.1232**	**−12.3079**	**129.7919**	**0.99239**
T2	153.8509	158.3029	158.2985	3(5–7)	46.6243	**6(8–9)**	**0.033109**	**−80.3194**	**1.0949**	**−4.7272**	**75.2952**	**1.0211**
T3	172.6368	173.2049	179.0808	8(9–6)	76.0102	**9(6–4)**	**0.081204**	**−36.5941**	**1.2133**	**−3.8975**	**196.7476**	**1.0205**
T4	181.0729	187.3188	187.3783	3(5–7)	38.9587	**6(8–9)**	**0.055718**	**−39.4788**	**1.1083**	**1.1078**	**93.9452**	**1.0158**
T5	64.404	68.0017	74.8684	8(9–6)	80	**3(5–7)**	**0.05307**	**−139.996**	**1.1861**	**−0.25645**	**127.1139**	**1.067**
T6	158.7672	168.8062	171.7629	9(6–4)	80	**8(9–6)**	**0.03401**	**−98.5713**	**1.311**	**−13.9009**	**240.9063**	**1.09**
T7	151.8813	157.6258	157.9015	5(7–8)	57.2176	**8(9–6)**	**0.084799**	**49.2865**	**1.2148**	**9.9574**	**162.9652**	**1.0613**
T8	101.546	102.9787	104.0963	8(9–6)	57.3979	**9(6–4)**	**0.044498**	**−111.54**	**1.1522**	**−1.3824**	**138.5147**	**1.0159**
T9	79.5977	83.315	82.1687	3(5–7)	65.3655	**2(4–5)**	**0.078229**	**−155.026**	**1.208**	**−0.84122**	**139.3665**	**1.0788**
T10	172.052	178.886	178.3593	8(9–6)	35.0626	**2(4–5)**	**0.050238**	**35.9756**	**1.2966**	**−3.8205**	**233.5245**	**1.0805**

Table 10 Enhanced ATC values with TCSC–UPFC under coordination $Scheme_3$

Trans. ID	ATC, MW TCSC only	ATC, MW UPFC only	TCSC-UPFC	TCSC's solution Line no.	TCSC's solution % comp	UPFC's solution Line no.	UPFC's solution V_{se}, p.u	UPFC's solution δ_{se}, deg	UPFC's solution V_{sh}, p.u	UPFC's solution δ_{sh}, deg	UPFC's solution Q_{sh} (MVAR)	UPFC's solution V_{sh}^{b}, p.u
T1	182.0445	220.262	226.5575	8(9–6)	**80**	**3(5–7)**	**0.1**	**−87.9262**	**1.1208**	**−12.2847**	**129.6178**	**0.98983**
T2	153.8509	158.3029	158.3021	3(5–7)	**14.6875**	**5(7–8)**	**0.084404**	**101.9834**	**1.0742**	**8.142**	**50.4921**	**1.025**
T3	172.6368	173.2049	179.0898	8(9–6)	**63.8201**	**9(6–4)**	**0.087222**	**−8.6794**	**1.2317**	**−5.8501**	**207.6833**	**1.0301**
T4	181.0729	187.3188	187.4344	3(5–7)	**10.9356**	**8(9–6)**	**0.039868**	**39.3922**	**1.2821**	**6.1253**	**221.8501**	**1.0759**
T5	64.404	68.0017	74.8387	8(9–6)	**80**	**3(5–7)**	**0.041902**	**−112.593**	**1.1419**	**−0.0935**	**104.1517**	**1.0419**
T6	158.7672	168.8062	171.7609	9(6–4)	**80**	**8(9–6)**	**0.034119**	**−98.6956**	**1.311**	**−13.8976**	**240.8763**	**1.09**
T7	151.8813	157.6258	157.8904	5(7–8)	**80**	**8(9–6)**	**0.066189**	**27.4105**	**1.1935**	**11.8533**	**146.6745**	**1.0544**
T8	101.546	102.9787	104.0963	8(9–6)	**65.797**	**9(6–4)**	**0.068583**	**−104.516**	**1.1468**	**0.064611**	**137.6198**	**1.0107**
T9	79.5977	83.315	83.3153	3(5–7)	**9.2573**	**5(7–8)**	**0.02718**	**143.0659**	**1.0659**	**14.9146**	**41.9045**	**1.0251**
T10	172.052	178.886	179.129	8(9–6)	**50.1268**	**5(7–8)**	**0.1**	**94.0623**	**1.0782**	**9.1945**	**54.5103**	**1.025**

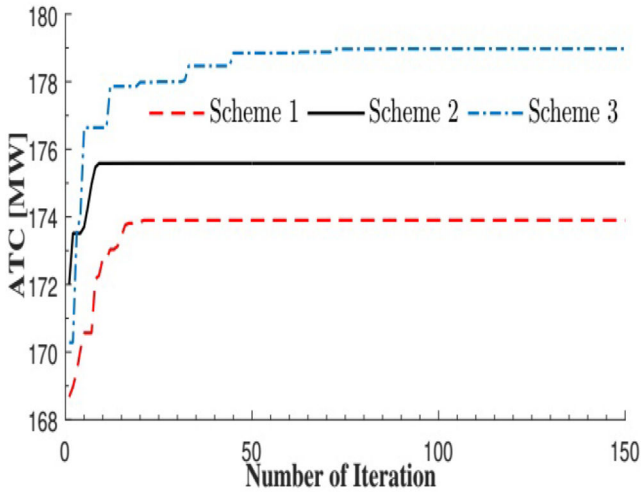

Fig. 15 *Coordination schemes comparison for transaction T3*

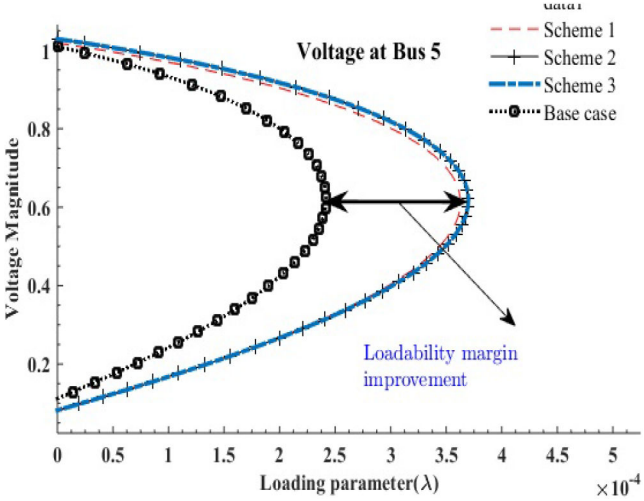

Fig. 16 *Complete nose curves of transaction T1*

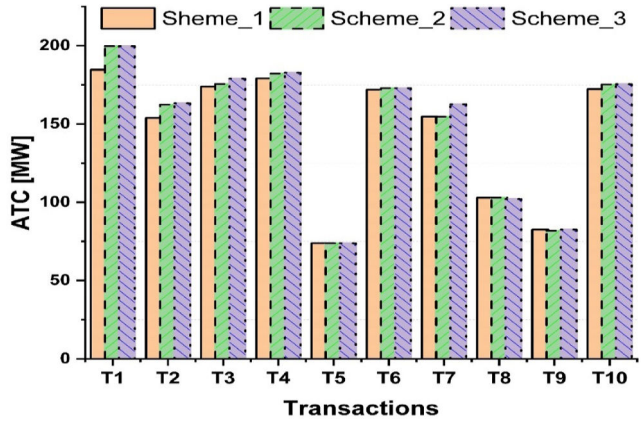

Fig. 17 *TCSC–SSSC-based comparison of coordination schemes*

parameters ($X_{TCSC}, \lambda_{SSSC}, X_{SSSC}$) required to be optimally tuned simultaneously.

Since power systems loadability improvement is a measure of transfer capability, consequently Fig. 16 compares the nose curves of all schemes under TCSC–SSSC coordination for transactions T1. Again, as shown in Tables 5–10, as well as Fig. 16, coordination of $scheme_2$ and $scheme_3$, gives higher loadability margin compared to $scheme_1$ and the base case without FACTS.

For TCSC–SSSC and TCSC–UPFC, respectively, Figs. 17 and 18 depict a comparison amongst the multi-type FACTS coordination schemes. Fig. 17 illustrates that $scheme_2$ and $scheme_3$

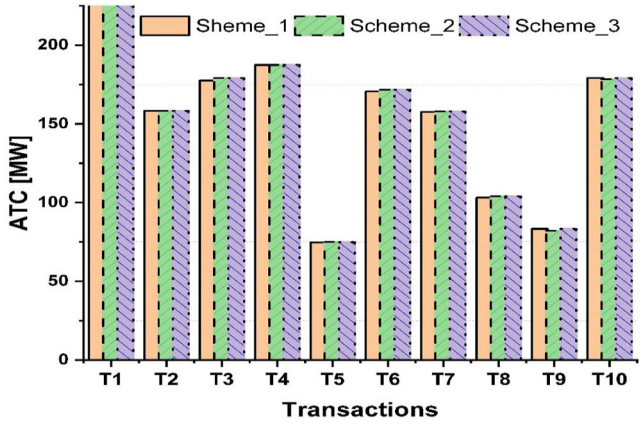

Fig. 18 *TCSC–UPFC-based comparison of coordination schemes*

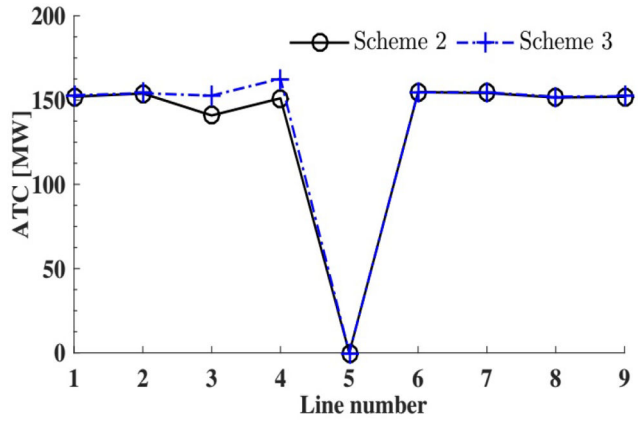

Fig. 19 *Comparison of coordination schemes for transaction T5*

are competing for the superior ATC, particularly in transactions T1–T4 under the TCSC–SSSC.

To further examine the superiority of the coordination schemes in obtaining superior ATC, Fig. 19 compares the ATC by coordination $scheme_2$ and $scheme_3$ for an exhaustive search at all locations for transaction T5 under the TCSC–SSSC coordination scenario. Although both schemes follow the same pattern of ATC improvement at each location, $scheme_3$ obtains greater improvement at line number 4, which is consistent with the results of Table 7. The zero ATC value in line number 5 of Fig. 19 is a result of non-placement of SSSC at the same location with an existing TCSC.

Additionally, Fig. 20 depicts a surface plot of ATC values for both multi-type FACTS coordination, a comparison of TCSC–SSSC and TCSC–UPFC in Figs. 17 and 18, and as depicted in Fig. 20 shows that depending on the transaction, in general, the TCSC–UPFC coordination obtains the superior ATC values, particularly for transactions T1, T3, T4, T5, T8, T9, and T10. The higher ATC obtained by TCSC–UPFC compared to TCSC–SSSC is attributed to the presence of the UPFC devices compared with the SSSC. Since the UPFC has two VSC; at the line of insertion, the UPFC simultaneously has impacts on both the series and shunt branches as depicted in Fig. 7. Therefore, apart from the injection by the series converter in the SSSC, the UPFC's shunt converter injection contributes to power flow redistribution and hence relief congestion and improve the voltage profile particularly at the shunt branch.

Moreover, in Fig. 20, for transaction T1, it is observed that the three coordination schemes obtain ATC of about 226.5577 MW under the TCSC–UPFC coordination, which represents about 58% improvement. Similarly, for transaction T5, the TCSC–SSSC and TCSC–UPFC achieved 69.34 and 71.59%, respectively.

8 Conclusion

The main objective of the work which demonstrates the optimal location and coordination of multi-type FACTS is achieved under

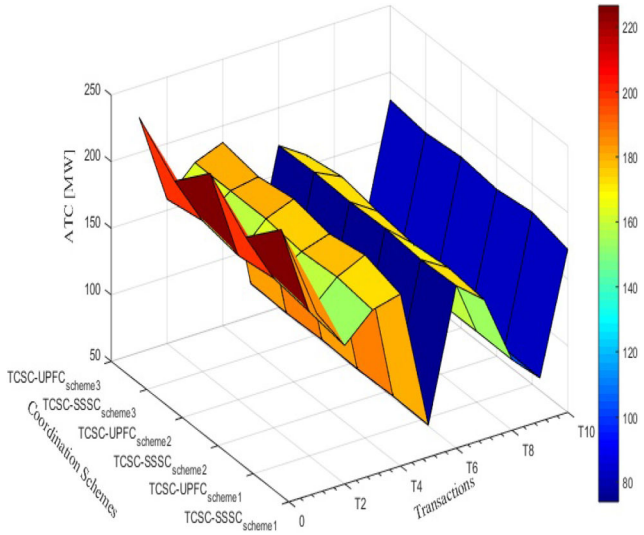

Fig. 20 *Surface plot of ATC values obtained by all of the coordination schemes*

different time horizons. Two multi-type FACTS coordinations namely TCSC-SSSC and TCSC-UPFC were illustrated. The approach deploys a hybrid real power flow PI and particle swarm optimisation (PI–PSO). The main results obtained show that compared to conventional PSO, PI–PSO performs better regarding exploitation, thereby improve the starting point, enhanced ATC, and reduce the number of iterations to the optimal solution. Moreover, PI–PSO avoids local optimal solutions, a characteristic observed in the conventional PSO. Furthermore, TCSC–UPFC coordination improves the overall loadability and ATC compared to TCSC–SSSC. Also, a comparison of the various coordinations, $scheme_1$, $scheme_2$, and $scheme_3$, indicates that the coordination scheme with a higher number of optimisation decision parameters ($scheme_3$) give superior ATC values with multi-type FACTS coordination. Though the power transfer directions considered were all constraints by line overloads at base case, future work intends to address transactions limited by bus voltage as well as examine the use of PI–PSO with $(N-1)$ contingency considerations.

9 References

[1] Chen, H., Fang, X., Zhang, R., *et al.*: 'Available transfer capability evaluation in a deregulated electricity market considering correlated wind power', *IET Gener. Transm. Distrib.*, 2018, **12**, (1), pp. 53–61

[2] Jain, T., Singh, S.N., Srivastava, S.C.: 'Dynamic available transfer capability computation using a hybrid approach', *IET Gener. Transm. Distrib.*, 2008, **2**, (6), pp. 775–778

[3] Sutha, S., Kamaraj, N.: 'Optimal location of multi type facts devices for multiple contingencies using particle swarm optimization', *Int. J. Electr. Comput. Energ. Electron. Commun. Eng.*, 2008, **2**, (10), pp. 2275–2281

[4] Surya, R., Janathanan, N., Balamurugan, S.: 'A novel technique for congestion management in transmission system by real power flow control'. Proc. Int. Conf. on Intelligent Computing, Instrumentation and Control Technologies (ICICICT), Kannur, India, July 2017, pp. 1349–1354

[5] Kulkarni, P.P., Ghawghawe, N.D.: 'Optimal placement and parameter setting of TCSC in power transmission system to increase the power transfer capability'. Proc. Int. Conf. on Energy Systems and Applications (ICESA 2015), Pune, India, October–November 2015, pp. 735–739

[6] Mohamed, S.A., Luo, N., Pujol, T., *et al.*: 'Voltage sourced converter (VSC) based on multiple FACTS controllers for the improvement of power quality', *Renew. Energy Power Qual. J.*, 2018, **1**, (16), pp. 65–70

[7] Salim, N.A., Othman, M.M., Serwan, M.S., *et al.*: 'Determination of available transfer capability with implication of cascading collapse uncertainty', *IET Gener. Transm. Distrib.*, 2014, **8**, (4), pp. 705–715

[8] Li, G., Lie, T.T., Shrestha, G.B., *et al.*: 'Design and application of co-ordinated multiple FACTS controllers', *IET Gener. Transm. Distrib.*, 2000, **147**, (2), pp. 112–118

[9] Van-Hertem, D., Eriksson, R., Soder, L., *et al.*: 'Coordination of multiple power flow controlling devices in transmission systems'. Proc. 9th IET Int. Conf. on AC and DC Power Transmission (ACDC 2010), London, UK, October 2010, pp. 1–6

[10] Li, C., Xiao, L., Cao, Y., *et al.*: 'Optimal allocation of multi-type FACTS devices in power systems based on power flow entropy', *J. Mod. Power Syst. Clean Energy*, 2014, **2**, (2), pp. 173–180

[11] Elmitwally, A., Eladl, A.: 'Planning of multi-type FACTS devices in restructured power systems with wind generation', *Int. J. Electr. Power Energy Syst.*, 2016, **77**, (1), pp. 33–42

[12] Singh, B., Sharma, N.K., Tiwari, A.N., *et al.*: 'Enhancement of voltage stability by coordinated control of multiple FACTS controllers in multi-machine power system environments'. Proc. Int. Conf. on Sustainable Energy and Intelligent Systems (SEISCON 2011), Chennai, India, July 2011, pp. 18–25

[13] Li, C., Kong, D., Xue, Y., *et al.*: 'Enhancement of power system small-signal stability by coordinated damping control of multiple FACTS devices'. Proc. 13th IET Int. Conf. on AC and DC Power Transmission (ACDC 2017), Manchester, UK, February 2017, pp. 1–6

[14] Ghahremani, E., Kamwa, I.: 'Optimal placement of multiple-type FACTS devices to maximize power system loadability using a generic graphical user interface', *IEEE Trans. Power Syst.*, 2013, **28**, (2), pp. 764–778

[15] Chansareewittaya, S., Jirapong, P.: 'Total transfer capability enhancement with optimal number of UPFC using hybrid TSSA'. Proc. 9th Int. Conf. on Electrical Engineering/Electronics, Computer, Telecommunications and Information Technology (ECTI-CON 2012), Phetchaburi, Thailand, May 2012, pp. 1–4

[16] Nireekshana, T., Kesava, G.R., Sivanaga, S.R.: 'Available transfer capability enhancement with FACTS using cat swarm optimization', *Ain Shams Eng. J.*, 2016, **7**, (1), pp. 159–167

[17] Idris, R.M., Kharuddin, A., Mustafa, M.W.: 'Optimal allocation of FACTS devices for ATC enhancement using bees algorithm', *Int. J. Electr. Comput. Energ. Electron. Commun. Eng.*, 2009, **3**, (6), pp. 1295–1302

[18] Chansareewittaya, S., Jirapong, P.: 'Power transfer capability enhancement with optimal maximum number of FACTS controllers using evolutionary programming'. Proc. 37th Annual Conf. of the IEEE Industrial Electronics Society (IECON 2011), Melbourne, VIC, Australia, November 2011, pp. 4733–4738

[19] Jamnani, J.G., Pandya, M.: 'Coordination of SVC and TCSC for management of power flow by particle swarm optimization', *Energy Procedia*, 2019, **156**, (1), pp. 321–326

[20] Nadeem, M., Kashif, I., Abraiz, K., *et al.*: 'Optimal placement, sizing and coordination of FACTS devices in transmission network using whale optimization algorithm', *Energies*, 2020, **13**, (753), pp. 1–24

[21] Chansareewittaya, S., Jirapong, P.: 'Optimal allocation of multi-type FACTS controllers for total transfer capability enhancement using hybrid particle swarm optimization'. Proc. IEEE 11th Int. Conf. on Electrical Engineering/Electronics, Computer, Telecommunications and Information Technology (ECTI-CON), Nakhon Ratchasima, Thailand, May 2014, pp. 1–6

[22] Bavithra, K., Raja, S.C., Venkatesh, P.: 'Optimal setting of FACTS devices using particle swarm optimization for ATC enhancement in deregulated power system', *IFAC-PapersOnLine*, 2016, **49**, (1), pp. 450–455

[23] Sadiq, A.A., Buhari, M., Adamu, S.S.: 'Multi-type FACTS location and coordination using PI–PSO for transfer capability improvement'. Proc. IEEE PES/IAS PowerAfrica, Abuja, Nigeria, August 2019, pp. 662–667

[24] Srinivasa V, V.R., Srinivasa R, R.: 'Comparison of various methods for optimal placement of FACTS devices'. Int. Conf. on Smart Electric Grid (ISEG) 2014, Guntur, India, 19–20 September 2014, no. 1, pp. 1–7

[25] Ebeed, M., Kamel, S., Jurado, F.: 'Constraints violation handling of SSSC with multi-control modes in newton-raphson load flow algorithm', *IEEJ Trans. Electr. Electron. Eng.*, 2017, **12**, (6), pp. 861–866

[26] Zhang, X.P., Rehtanz, C., Pal, B.: '*Flexible AC transmission systems: modelling & control power systems*' (Springer, Verlag, Berlin, Heidelberg, 2006)

[27] Kamel, S., Jurado, F., Pecas-Lopes, J.A.: 'Comparison of various UPFC models for power flow control', *Electr. Power Syst. Res.*, 2015, **121**, (1), pp. 243–251

[28] Srinivasa, V.R., Srinivasa, R.R.: 'A generalized approach for determination of optimal location and performance analysis of FACTs devices', *Int. J. Electr. Power Energy Syst.*, 2015, **73**, (1), pp. 711–724

[29] Radman, G., Raje, R.S.: 'Power flow model/calculation for Power systems with multiple FACTS controllers', *Electr. Power Syst. Res.*, 2007, **77**, (12), pp. 1521–1531

[30] Haque, M.H., Yam, C.M.: 'A simple method of solving the controlled load flow problem of a power system in the presence of UPFC', *Electr. Power Syst. Res.*, 2003, **65**, (62), pp. 1–7
[31] Balasubbareddy, M., Sivanagaraju, S., Venkata, C.: 'A non-dominated sorting hybrid Cuckoo search algorithm for multi-objective optimization in the presence of FACTS devices', *Russ. Electr. Eng.*, 2017, **88**, (1), pp. 44–53
[32] Manikandan, S., Arul, P.: 'Optimal location of multiple FACTS device using sensitivity methods', *Int. J. Eng. Trends Technol.*, 2013, **4**, (10), pp. 4361–4367
[33] Lubis, R.S., Hadi, S.P., Tumiran, : 'Using the UPFC and GUPFC controllers to maximize available transfer capability (ATC)', *Int. J. Electr. Eng. Inf.*, 2014, **6**, (2), pp. 374–393
[34] Sadiq, A.A., Adamu, S.S., Buhari, M.: 'Available transfer capability enhancement with FACTS using hybrid PI-PSO', *Turkish J. Electr. Eng. Comput. Sci.*, 2019, **27**, (4), pp. 2881–2897
[35] Yao, R., Liu, F., He, G.*, et al.*: 'Static security region calculation with improved CPF considering generation regulation'. Proc. IEEE Int. Conf. on Power System Technology (POWERCON 2012), Auckland, New Zealand, October–November 2012, pp. 1–6
[36] Dou, X., Zhang, S., Chang, L.*, et al.*: 'An improved CPF for static stability analysis of distribution systems with high DG penetration', *Int. J. Electr. Power Energy Syst.*, 2017, **86**, (3), pp. 177–188
[37] Khosravifard, M., Shaaban, M.: 'Risk-based available transfer capability assessment including nondispatchable wind generation', *Int. Trans. Electr. Energy Syst.*, 2015, **25**, (11), pp. 3169–3183
[38] Babulal, C.K., Kannan, P.S.: 'A novel approach for ATC computation in deregulated environment', *J. Electr. Syst.*, 2006, **2**, (3), pp. 146–161
[39] Prathiba, R., Balasinghs, M.M., Devaraj, D.*, et al.*: 'Multiple output radial basis function neural network with reduced input features for on-line estimation of available transfer capability', *Control Eng. Appl. Inf.*, 2016, **18**, (1), pp. 95–106
[40] Zimmerman, R.D., Murillo-Sanchez, C.E., Thomas, R.J.: 'MATPOWER: steady-state operations, planning, and analysis tools for power systems research and education', *IEEE Trans. Power Syst.*, 2011, **26**, (1), pp. 12–19